Chapter 5

Numerical Simulation Methods Applied at Fiber Grating Sensors Design

Dan Savastru, Sorin Miclos, Marina Tautan and
Ion Lancranjan

Additional information is available at the end of the chapter

http://dx.doi.org/10.5772/63890

Abstract

The paper presents the results obtained in simulation of fiber Bragg grating (FBG) and long-period grating (LPG) sensors and their applications. The optical properties of FBG and LPG are firstly analyzed and, consequently, the basics of simulation models are provided. Coupled-mode theory and the transfer matrix methods are the two techniques used for the simulation of FBG and LPG. The numerical simulations are performed for an improved design of these types of fiber sensors, designs dedicated to specified applications. The different FBG types, i.e. the normal, chirped, apodized, according to different laws and tilted cases, are analyzed. Also, various LPG configurations are numerically simulated. The two main categories of sensing applications, for temperature and for mechanical stress/strain evaluation, are simulated for each type of fiber grating sensor. The chapter is intended to be a synthesis of already obtained results to which some results of research in development are added.

Keywords: Distributed feedback devices, Optical fibers, Fiber gratings, Fiber Bragg grating, Long-period grating fiber, Optical fiber communication, Optical fiber devices, Optical fiber filters

1. Introduction

Into an increasing number of scientific, medical, industrial and military sensing and telecommunication applications, optic fibers are used, which have a spatial periodic variation of the refractive index inscribed in the core, δn, periodic variation defined as grating, the fiber optic being denoted under the general name "fiber grating" [1–5]. There are two main types of such

optic fibers: the fiber Bragg grating (FBG) ones and the long-period grating (LPG) kind [5–7]. In literature, FBGs are considered as short-period grating (300–700 nm), while LPGs as long ones (10–1000 μm). For both FBGs and LPGs, the amplitude of the core refractive index is extremely small, in the range 0.0001–0.0005 or even smaller [5–12]. It is important to mention that only step index optic fibers for which the weakly guiding approximation relying on a very small difference between the values of the core and cladding refractive index, n_{co}–n_{cl}, is applicable are analyzed [5–7, 11–15]. Related to this, it has to be underlined the fact that the amplitude of the spatial periodic variation of the refractive index inscribed in the core is smaller than n_{co}–n_{cl} [11–15]. The basic functions as sensors and/or wavelength filter of both FBG and LPG are accomplished by controlled, observed and measured variations of optical fiber refractive indexes of the core (n_{co}) and cladding (n_{cl}) to which the refractive index of the ambient (n_{amb}) is added, where the optical fiber is mounted. Consequently, the spectral characteristics that can be observed in fiber reflection (FBG) and transmission (LPG) gratings will be described [13–19]. For an improved design of experimental setups dedicated to the above-mentioned applications, it is obvious that, for both FBG and LPG, the principles for understanding and tools for designing fiber gratings are emphasized [11–20]. The emphasized understanding principles and designing tools are applicable for the wide variety of optical properties that are possible in fiber gratings [19–28]. There are given examples related to the large number of fiber grating subtypes of both FBG and LPG, considering uniform, apodized, chirped, discrete phase-shifted and superstructure gratings; symmetric and tilted gratings; and cladding-mode and radiation-mode coupling gratings [20–33].

Both FBGs and LPGs are manufactured in single-mode silicate optic fiber by modifying in a periodic manner its core refractive index using UV-irradiation delivered by Ar or other UV laser [20]. Most commonly, the LPG is created by altering the core in a periodic manner, but another class of manufacturing methods physically deforms the fiber to create the required optical modulation [34–40]. These include the following: irradiation from a carbon dioxide laser, radiation with femtosecond pulses and writing by electric discharge, ion implantation, periodic ablation and/or annealing, corrugation of the cladding, micro-structuring of tapered fibers and dopant diffusion into the fiber core.

2. Theory

This section presents the optical properties of FBG and LPG. Consequently, the basics of simulation models are provided. Coupled-mode theory and the transfer matrix methods are the two techniques used for the simulation of FBG and LPG [13, 14, 17, 20, 22–28]. Thus, the physical mechanism of the grating electric field interaction is given and aims to provide the reader with insight into the operation principles of FBG and LPG. The gratings are inscribed into the core of a step index optic fiber; consequently, the step index optic fiber case is analyzed.

Optical fiber mainly consists of a core, cladding and a protective layer called the primary plastic buffer coating. The optical fiber acts as a waveguide for optical frequencies and is normally cylindrical in shape. The core is a dielectric cylinder surrounded by the cladding to form a

http://dx.doi.org/10.5772/63890

larger dielectric cylinder [13, 14]. The optical fiber has a uniform refractive index up to the core-cladding conjunction, where it undergoes a sharp change in refractive index. The refractive index of the core and the cladding is given as n_{co} and n_{cl}, respectively, the relation $n_{co} > n_{cl}$ being valid [13, 36, 37]. This is the necessary condition for total internal reflection to occur. The structure and material of the fiber confines the electromagnetic waves to a direction parallel to the axis and also affects the transmission properties of the optic fiber [13, 20]. The light transmitted through the fiber is confined due to total internal reflection within the material. There are practically no electromagnetic fields outside the cladding because of exponential decay within this region [13]. The difference between n_{co} and n_{cl} is very small, of 10^{-4} order. This is the necessary condition for the weakly guiding approximation to be applicable. This approximation results into a mathematical apparatus, which allows description of fiber grating processes as a byproduct. **Figure 1** shows the schematics of a typical optical fiber layout. For a single-mode step index fiber commonly used for grating to be inscribed into the core, the core radius is in the range 1.5–5 μm, the cladding radius being typically of 62.5 μm.

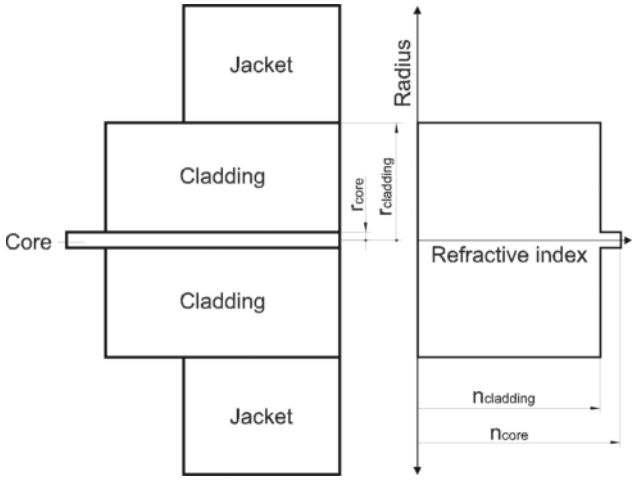

Figure 1. The schematics of a typical optical fiber layout.

It is assumed that a perturbation to the effective refractive index of the guided mode(s) can be defined as follows [13]:

$$\delta n_{eff}(z) = \delta n_{effmean}(z)\left\{1 + v \cdot \cos\left[\frac{2\pi}{\Lambda} z + \varphi(z)\right]\right\} \quad (1)$$

where $\delta n_{effmean}$ is the amplitude of the perturbation, evaluated as the index change spatially averaged on a grating period, v is the fringe visibility of the index change, Λ is the nominal period and $\varphi(z)$ is the grating chirp, which represents a variation of nominal period. In the case

of a step index fiber without a grating, the core power confinement factor, Γ, is defined. For uniformity across the core-induced grating, with an induced index change δn_{co} created in core, for the propagation mode, the following relation is defined [13, 21–28, 36]:

$$\delta n_{eff} \cong \Gamma \cdot \delta n_{co} \tag{2}$$

Since FBG or LPG is manufactured starting from single-mode light is propagating along the core as LP_{01} modes for which an effective index parameter b is introduced. It is useful to introduce the normalized frequency, V, a parameter synthetically characterizing the geometrical and optical materials fiber properties [13, 36, 37]. V is defined as follows:

$$V = \left(\frac{2\pi}{\lambda}\right) \cdot a_{co} \cdot \sqrt{n_{co}^2 - n_{cl}^2} \tag{3}$$

where a_{co} is the core radius. The effective index parameter is a solution to the dispersion relation [20]:

$$V\sqrt{1-b} \cdot \frac{J_{l-1}\left(V\sqrt{1-b}\right)}{J_l\left(V\sqrt{1-b}\right)} = -V\sqrt{b} \cdot \frac{K_{l-1}\left(V\sqrt{b}\right)}{K_l\left(V\sqrt{b}\right)} \tag{4}$$

where l is the Azimuthal order of the mode LP_{01}. In Eq. (4), J_l are the Bessel functions of the first kind and K_l are the modified Bessel functions of the second kind. The effective index n_{eff} is related to through the relation [13, 20–28]:

$$b = \frac{n_{eff}^2 - n_{cl}^2}{n_{co}^2 - n_{cl}^2} \tag{5}$$

Once b and V are known, Γ can be determined from

$$\Gamma = \frac{b^2}{V^2}\left[1 - \frac{J_l^2\left(V\sqrt{1-b}\right)}{J_{l+1}\left(V\sqrt{1-b}\right)J_{l-1}\left(V\sqrt{1-b}\right)}\right] \tag{6}$$

A fiber grating, FBG or LPG, is the periodic variation of refractive index within the core of a step index single-mode optical fiber. In **Figures 2** and **3**, the schematics of the two considered types of an optical fiber with a grating written in the core of the fiber are shown. The core inscribed refractive index changes can be described as cylinders. The refractive index changes

http://dx.doi.org/10.5772/63890

of a fiber grating usually have a near sinusoidal variation. Firstly, the simple case of a uniform grating fiber grating is considered.

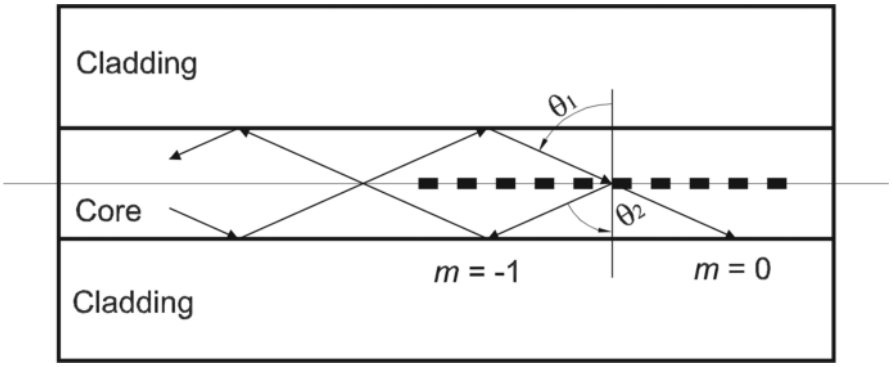

Figure 2. Propagation in a FBG.

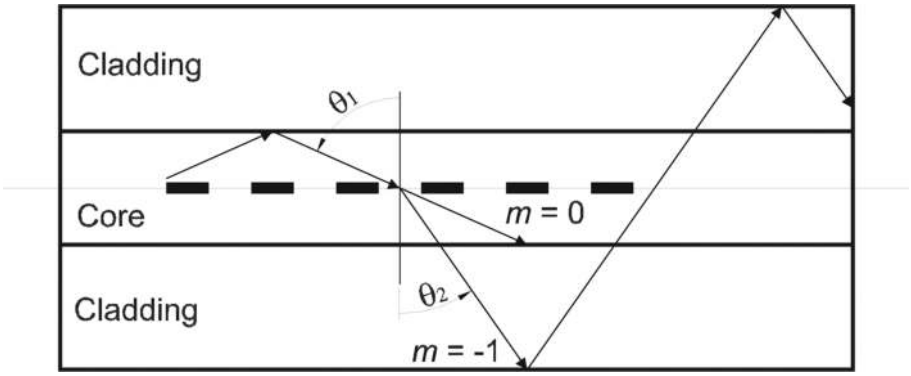

Figure 3. Propagation in a LPG.

A fiber grating produces coupling between two fiber modes [13, 14, 20, 21]. The quantitative analysis of this phenomenon is achieved using coupled-mode theory. It is helpful to consider a qualitative analysis of the basic interactions of interest. A fiber grating is simply an optical diffraction grating, at each refractive index change junction, refraction and reflection occur, and thus its effect upon a light wave incident on it can be described by the familiar grating equation. The diffraction of the light incident on the diffraction grating at an angle θ_1 can be described by the equation from Snell's law [13, 14]:

$$n \cdot \sin\theta_2 = n \cdot \sin\theta_1 + m \cdot \frac{\lambda}{\Lambda} \tag{7}$$

where m determines the diffraction order and θ_2 is the angle of the diffracted wave λ and ^ are the wavelength of the incident light and the period of the diffraction grating, respectively. Eq. (6) can predict only the directions θ_2 into which constructive interference occurs, but it is not useful for determining the wavelength at which a fiber grating most efficiently couples light between two modes.

A fiber grating's main function is based on coupling between the modes propagating through the fiber, modes which can travel in opposite directions or in the same direction—this being the basic criterion for classification of fiber gratings into two main types: (a) modes traveling in the opposite directions, denoted as the short-period gratings, the fiber Bragg gratings (FBG), working as the reflection gratings; (b) modes traveling in the same direction, denoted as Long-Period Gratings (LPG), working as transmission gratings.

In **Figure 2**, the mode reflection by a Bragg grating is schematically presented. The incident mode has a bounce angle of θ_2 and becomes the same mode traveling in the opposite direction with a bounce angle of $\theta_2 = - \theta_1$. It is worth to underline that the entire process is taking place only inside the core. For the incident and diffracted rays, the propagation constants are calculated as follows [13, 14]:

$$\begin{aligned} \beta_1 &= \frac{2\pi}{\lambda} n_{eff1}\ ,\ n_{eff1} = n_{co} \sin\theta_1 \Rightarrow \beta_1 = \left(\frac{2\pi}{\lambda}\right) n_{co} \sin\theta_1 \\ \beta_2 &= \frac{2\pi}{\lambda} n_{eff2}\ ,\ n_{eff2} = n_{co} \sin\theta_2 \Rightarrow \beta_2 = \left(\frac{2\pi}{\lambda}\right) n_{co} \sin\theta_2 \end{aligned} \tag{8}$$

Eq. (7) can be rewritten in terms of the propagation constant of the incident beam and the reflected/diffracted light as follows [13, 14, 20–28]:

$$\beta_2 = \beta_1 + m\frac{2\pi}{\Lambda} \tag{9}$$

where the subscripts 1 and 2 describe the incident and reflected/diffracted propagation constant. For first-order diffraction, which usually dominates in a fiber grating, $m = -1$. Eq. (9) is modified to [13, 14, 20]

$$\beta_2 = \beta_1 - \frac{\lambda}{\Lambda} \tag{10}$$

For the bound core modes, the following relation is fulfilled:

$$n_{cl} < n_{eff} < n_{co} \tag{11}$$

http://dx.doi.org/10.5772/63890

In order to be rigorous, for the cladding modes, a relation similar to Eq. (11) is obtained by considering the value of optic fiber ambient medium, usually air, refractive index:

$$1 < n_{eff} < n_{cl} \tag{12}$$

Fiber modes that propagate in the negative (−z) direction are described by negative β values. Using Eq. (9) and observing that $\beta_2 < 0$, the resonant wavelength is obtained for reflection of a mode of index n_{eff1} into reflection of a mode of index n_{eff2} as defined by the relation:

$$\lambda = \left(n_{eff\,1} + n_{eff\,2}\right) \cdot \Lambda \tag{13}$$

Normally, the two counter propagating fiber modes have propagation constants with the same absolute value and the following relation is defined:

$$n_{eff} = n_{eff\,1} = n_{eff\,2} \tag{14}$$

From (14), the familiar result for Bragg reflection peak wavelength is obtained:

$$\lambda_B = 2 \cdot n_{eff} \cdot \Lambda \tag{15}$$

In **Figure 3**, the diffraction is schematically presented by a transmission of a fiber core mode with a bounce angle θ_1 on the grating into a cladding co-propagating fiber mode with an angle θ_2 [13, 14, 20–28]. Since, in the case illustrated in **Figure 1**, both incident core and transmitted cladding fiber modes propagate in positive +z direction, it follows that β ‼ 0. As a consequence, Eq. (9) predicts the resonant wavelength of an absorption peak for a transmission grating as follows:

$$\lambda = \left(n_{eff\,1} - n_{eff\,2}\right) \cdot \Lambda \tag{16}$$

The Bragg condition required for a (fundamental) mode to couple to another mode (backward propagating or forward propagating) results from two requirements [20, 21]:

1. Energy conservation. It means that the frequency of the incident and reflected radiation is constant—no wavelength shift is observed because of reflection.
2. Momentum conservation. It means that the wave vector of the scattered radiation $\vec{k}_f$ is equal to the sum of the incident wave vector $\vec{k}_i$ and the grating wave vector $\vec{K}$

$$\vec{K} + \vec{k}_i = \vec{k}_f \tag{17}$$

$$K = \left|\vec{K}\right| = \frac{2\pi}{\Lambda} \tag{18}$$

Coupled-mode theory is used for quantitative information about the diffraction efficiency and spectral characteristics of fiber gratings by assuming the approximation of a weakly guiding fiber [13, 14, 36, 37]. Implicitly, it is assumed that the propagating fiber modes have slowly varying along the *z* direction amplitudes. Also it is assumed that a fiber mode has a transverse component of the electric field defined as a superposition of the modes labeled "*j*" traveling in the +*z* and −*z* directions such that [13, 20, 36]

$$\vec{E}_t(x,y,z,t) = \sum_j \left[A_j(z)\exp\left(i\beta_j z\right) + B_j(z)\exp\left(-i\beta_j z\right)\right]\cdot \vec{e}_{jt}(x,y)\exp\left(-i\omega t\right) \tag{19}$$

where $A_j(z)$ and $B_j(z)$ are slowly varying amplitudes of the j^{th} mode, respectively. Eq. (19) describes the transverse mode electric fields of the bound core or radiation LP_{il} modes, as given in [8], or of the cladding modes. Into an ideal uniform optical fiber, the modes are orthogonal and hence do not exchange energy; the presence of a dielectric perturbation such as a grating causes the modes to be coupled such that the amplitudes $A_j(z)$ and $B_j(z)$ of the *j*th mode evolution along the *z* axis are defined according to

$$\frac{dA_j}{dz} = i\sum_k A_k\left(K_{kj}^t + K_{kj}^z\right)\exp\left[i\left(\beta_k - \beta_j\right)z\right] + i\sum_k B_k\left(K_{kj}^t - K_{kj}^z\right)\exp\left[-i\left(\beta_k + \beta_j\right)z\right] \tag{20}$$

$$\frac{dB_j}{dz} = -i\sum_k A_k\left(K_{kj}^t - K_{kj}^z\right)\exp\left[i\left(\beta_k + \beta_j\right)z\right] - i\sum_k B_k\left(K_{kj}^t + K_{kj}^z\right)\exp\left[-i\left(\beta_k - \beta_j\right)z\right] \tag{21}$$

In (20) and (21), two coupling coefficients are introduced: transverse and longitudinal. The transverse coupling coefficient between modes *k* and *j* is given by

$$K_{kj}^t(z) = \frac{\omega}{4}\iint_\infty dxdy\Delta\varepsilon(x,y,z)\cdot\vec{e}_{kt}(x,y)\cdot\vec{e}_{jt}^{\,*}(x,y) \tag{22}$$

where Δ ε is the perturbation to the electric permittivity, which has a very small value in the weakly guiding approximation. When $\delta n << n$, the Δ ε perturbation can be approximated as $\Delta\varepsilon \cong 2n\delta n$. The longitudinal coupling coefficient $K_{kj}^z(z)$ is analogous to $K_{kj}^t(z)$, but for slow

http://dx.doi.org/10.5772/63890

longitudinally varying fiber modes approximation, the condition $K_{kj}^{z}(z) << K_{kj}^{t}(z)$ is fulfilled and thus this coefficient is usually neglected.

In most fiber gratings, the induced index change δn (x, y, z)is approximately considered as uniform across the core and nonexistent outside the core. Thus, it becomes possible to define index by an expression similar to Eq. (1), but with $\delta n_{effmean}(z)$ replaced by $\delta n_{co}(z)$. As a consequence, it becomes convenient to define two new coefficients [13, 14, 20]

$$\sigma_{kj}(z) = \frac{\omega n_{co}}{2} \cdot \delta n_{comean}(z) \iint_{core} dxdy \cdot \vec{e}_{kt}(x,y) \cdot \vec{e}_{jt}^{*}(x,y) \tag{23}$$

$$\kappa_{kj}(z) = \frac{v}{2} \sigma_{kj}(z) \tag{24}$$

where σ is a "DC" (period-averaged) coupling coefficient and κ is an "AC" coupling coefficient, then the general coupling coefficient can be written as follows:

$$K_{kj}^{t}(z) = \sigma_{kj}(z) + 2\kappa_{kj}(z) \cdot \cos\left[\frac{2\pi}{\Lambda} z + \varphi(z)\right] \tag{25}$$

Eqs. (20)–(23) are the coupled-mode equations forming a set used to describe fiber grating spectra below.

2.1. FBG reflection spectra

In the FBG case, the dominant interaction in the fiber grating is the reflection of a mode $A(z)$ into an identical counter-propagating mode; at the Bragg resonance wavelength, Eqs. (20) and (21) are simplified by retaining only terms that involve the particular modes [13], neglecting terms on the right-hand sides of Eqs. (20) and (21) that contain rapidly oscillating z dependence, since these have low contributions to the variations of the mode amplitude. The resulting equations can be written as follows:

$$\frac{dR(z)}{dz} = i\hat{\sigma}R(z) + i\kappa S(z) \tag{26}$$

$$\frac{dS(z)}{dz} = -i\hat{\sigma}S(z) - i\kappa^{*}R(z) \tag{27}$$

In (26) and (27), as a starting hypothesis, it is assumed that $R(z)$ and $S(z)$ are defined as follows:

$$R(z) \equiv A(z) \cdot \exp\left(i\delta z - \frac{\varphi}{2} \right) \tag{28}$$

$$S(z) \equiv B(z) \cdot \exp\left(-i\delta z + \frac{\varphi}{2} \right) \tag{29}$$

In these equations, the "AC" coupling coefficient from (23) and the general "DC" self-coupling coefficient appear. The "AC" coupling coefficient is defined as follows:

$$\hat{\sigma} \equiv \delta + \sigma - \frac{1}{2}\frac{d\varphi}{dz} \tag{30}$$

The detuning δ, considered independent of z for all gratings, is defined as follows:

$$\delta \equiv \beta - \frac{\pi}{\Lambda} = \beta - \beta_D = 2\pi n_{eff}\left(\frac{1}{\lambda} - \frac{1}{\lambda_D} \right) \tag{31}$$

where λ_D is the "design wavelength" for Bragg scattering by an infinitesimally weak grating with a period $\delta n_{eff} \rightarrow$. The "design wavelength" λ_D is defined as follows:

$$\lambda_D = 2n_{eff}\Lambda \tag{32}$$

When $\delta = 0$, λ_D fulfill the Bragg condition, i.e. the following relation is accomplished

$$\lambda_D = \lambda_B \tag{33}$$

The "DC" coupling coefficient σ is defined in Eq. (23). Absorption loss in the grating is described by a complex coefficient $\hat{\sigma}$. The power loss coefficient α is the proportional to imaginary part of the complex coefficient $\hat{\sigma}$, being defined as follows:

$$\alpha = 2\,\mathrm{Im}(\sigma) \tag{34}$$

http://dx.doi.org/10.5772/63890

Light not reflected by the grating experiences a transmission loss *TL* expressed in dB/cm as follows:

$$TL = 10 \cdot \log_{10}(e)\alpha \tag{35}$$

The derivative describes possible chirp of the grating period, where φ(*z*) is defined using different variation laws. For a single-mode Bragg reflection grating, the following simple relations are useful:

$$\sigma = \frac{2\pi}{\lambda}\delta n_{effmean} \tag{36}$$

$$\kappa = \kappa^* \tag{37}$$

$$\hat{\sigma} = \frac{\pi}{\lambda} v \delta n_{effmean} \tag{38}$$

If the grating is uniform along *z*, then $\delta n_{effmean}$ is a constant, meaning no chirping of the grating, consequently $\frac{d\varphi}{dz}=0$, and thus κ, *σ* and $\hat{\sigma}$ are constants. Thus, Eqs. (26) and (27) form a system of coupled first-order ordinary differential equations with constant coefficients and appropriate boundary conditions for which closed-form solutions can be found. As the boundary conditions, for a grating of length *L*, it is assumed that a forward-going wave incident from *z* → -∞, the grating reflectivity, is unitary, *R*(*z*=-*L*/2)=1, and that no backward-going wave exists for *z* larger or equal to *L*/2, *S*(*z*=*L*/2)=0. The amplitude and power reflection coefficients ϱ and *r*, respectively, can then be shown to be defined as

$$\rho = \frac{-\kappa \sinh\left(L\sqrt{\kappa^2 - \hat{\sigma}^2}\right)}{\hat{\sigma}\sinh\left(L\sqrt{\kappa^2 - \hat{\sigma}^2}\right) + i\sqrt{\kappa^2 - \hat{\sigma}^2}\cosh\left(L\sqrt{\kappa^2 - \hat{\sigma}^2}\right)} \tag{39}$$

$$r = \frac{\sinh^2\left(L\sqrt{\kappa^2 - \hat{\sigma}^2}\right)}{\cosh^2\left(L\sqrt{\kappa^2 - \hat{\sigma}^2}\right) - \frac{\hat{\sigma}^2}{\kappa^2}} \tag{40}$$

From (40), it is found that the maximum reflectivity for a Bragg grating, r_{max}, is defined as

$$r_{\max} = \tanh^2(\kappa L) \tag{41}$$

This value occurs when $\hat{\sigma}=0$, or at the wavelength $\lambda_{\max}$, which is defined as

$$\lambda_{\max} = \left(1 + \frac{\delta n_{effmean}}{n_{eff}}\right)\lambda_D \tag{42}$$

2.2. LPG transmission spectra

In the LPG case, the coupled-mode equations are rearranged in the sense that near the peak resonance wavelength at which mode "1" of amplitude $A_1(z)$ is strongly coupled to a co-propagating mode "2" with amplitude $A_2(z)$, Eqs. (20) and (21) may be simplified by keeping only terms that involve the amplitudes of these two modes and then making use of the synchronous approximation of modes. The resulting equations can be written as follows:

$$\frac{dR(z)}{dz} = i\hat{\sigma}R(z) + i\kappa S(z) \tag{43}$$

$$\frac{dS(z)}{dz} = -i\hat{\sigma}S(z) + i\kappa^* R(z) \tag{44}$$

where the new amplitudes R(z) and S(z) are defined as

$$R(z) \equiv A_1 \exp\left[-i\frac{(\sigma_{11}+\sigma_{22})z}{2}\right]\exp\left(i\delta z - \frac{\varphi}{2}\right) \tag{45}$$

$$S(z) \equiv A_2 \exp\left[-i\frac{(\sigma_{11}+\sigma_{22})z}{2}\right]\exp\left(-i\delta z + \frac{\varphi}{2}\right) \tag{46}$$

and where $_{11}$ and $_{22}$ are "DC" coupling coefficients [13, 14]. From Eqs. (36), (37) and (38), the "AC" cross-coupling coefficient, κ, and, $\hat{\sigma}$, a general "DC" self-coupling coefficient are defined as

$$\kappa = \kappa_{21} = \kappa_{12}^* \tag{47}$$

http://dx.doi.org/10.5772/63890

and

$$\hat{\sigma} = \delta + \frac{\sigma_{11} - \sigma_{22}}{2} - \frac{1}{2}\frac{d\varphi}{dz} \tag{48}$$

Here the detuning, , which is assumed to be constant along z, is defined as

$$\delta \equiv \frac{1}{2}\left(\beta_1 - \beta_2\right) - \frac{\pi}{\Lambda} \tag{49}$$

or

$$\delta \equiv \pi \Delta n_{eff}\left(\frac{1}{\lambda} - \frac{1}{\lambda_D}\right) \tag{50}$$

In Eqs.(49) and (50), λ_D is the design wavelength for an infinitesimally weak grating; as for Bragg gratings, λ_D is defined as follows:

$$\lambda_D \equiv \Delta n_{eff} \Lambda \tag{51}$$

As for the Bragg grating case, δ = 0 corresponds to the grating resonance condition predicted by the qualitative picture of grating diffraction, schematically presented in **Figures 2** and **3**.

In the usual case of a uniform grating, $\hat{\sigma}$ and κ are constants. In the LPG case, unlike for a Bragg grating reflection of a single mode, here the coupling coefficient generally cannot be simply defined as in (38). For coupling between two different modes in the LPG case of transmission gratings, the overlap integrals (23) and (24) must be evaluated numerically. Like the analogous Bragg grating, Eqs. (43) and (44) are coupled first-order ordinary differential equations with constant coefficients. Thus, closed-form solutions can be found when appropriate initial conditions are specified for a grating of length L. The transmission can be found by assuming only one mode is incident from z → - ∞, and assuming that $R(0) = 1$ and $S(0) = 0$. The power bar and cross-transmission, $t_=$ and $t_\times$, respectively, can be defined as follows:

$$t_= = \frac{\left|R(z)\right|^2}{\left|R(0)\right|^2} = \cos\left(z\sqrt{\kappa^2 + \hat{\sigma}^2}\right) + \frac{\hat{\sigma}^2}{\hat{\sigma}^2 + \kappa^2}\sin\left(z\sqrt{\kappa^2 + \hat{\sigma}^2}\right) \tag{52}$$

$$t_{\times} = \frac{\left|S(z)\right|^2}{\left|R(0)\right|^2} = \frac{\kappa^2}{\hat{\sigma}^2 + \kappa^2} \sin\left(z\sqrt{\kappa^2 + \hat{\sigma}^2}\right) \tag{53}$$

The maximum cross-transmission (which occurs when $\hat{\sigma} = 0$) is defined as

$$t_{\times,\max} = \sin^2(\kappa L) \tag{54}$$

and it occurs at the wavelength

$$\lambda_{\max} = \frac{1}{1 - (\sigma_{11} - \sigma_{22})\frac{\Lambda}{2\pi}} \lambda_D \tag{55}$$

For coupling between a core mode "1" and a cladding mode "2" with an induced index change in the core only, $\sigma_{11} = \sigma$ from Eqs. (36), $\sigma_{22} \ll \sigma_{11}$and for low cladding confinement factor, $\lambda_{\max}$ can be approximated as

$$\lambda_{\max} \cong \left(1 + \frac{\delta n_{effmean}}{\Delta n_{eff}}\right) \lambda_D \tag{56}$$

In Eq. (56), it is assumed that $\delta n_{effmean}$, the induced change in the core-mode effective index, is much smaller than Δn_{eff} which is the common case. Analyzing Eqs. (56) and (42), a major difference is observed between the FBG and LPG cases, difference which consists in the fact that the wavelength of maximum coupling in a long-period cladding-mode coupler grating shifts toward longer wavelengths as the grating is being written many times more rapidly, meaning a longer grating period, than the shift occurring in the Bragg grating case.

3. Simulation results

Because of their various and important sensing and communication applications, the FBGs and LPGs are intensively studied in the last 20 years. Since the first reported results concerning their characteristics, fabrication and engineering their applications, in time, it became more and more clear that FBG and LPG simulation models are urgently needed for a proper design of their applications, especially the sensing ones. The design of FBG's and LPG's sensing applications involves a large number of input parameters or parameters having large variation

http://dx.doi.org/10.5772/63890

domains. In time, more or less accurate FBG and LPG simulation models were reported in literature [13, 14, 17, 20-28, 36-40]. These FBG and LPG simulation models are crucial for design of their applications.

However, in spite of the complicated mathematical apparatus defined in Section 2 used for describing the FBG or LPG mode of operation, there are several ideas which a researcher, using or designing FBG and LPG application, has to keep in mind:

1. The FBG and LPG applications are based on the fiber interaction with the environment. The FBG and LPG applications are developed starting by processing single mode fibers for grating formation.

2. In the FBG case, the whole process is taking place in the core of the optic fiber, without any direct interaction of the fiber grating with the environment. This means that only modes counter-propagating in pairs through the core are involved being coupled by the grating, i.e. exchanging energy. As a consequence, into the more or less broad emission spectrum of a light source connected at one end of the fiber, there will appear a reflection band which can be measured at the same fiber end or an absorption band as observed at the other fiber end. Usually, for the sake of spectroscopic measurements accuracy, the reflection band is mostly used. The peak wavelength and bandwidth of this band are the parameters of interest to be observed in applications. The main task of FBG simulations consists in defining the peak of the reflection band. The spectral shift of this peak wavelength of reflection band is correlated with grating period which can be modified by simple or simultaneous mechanical or thermal loads applied indirectly on the fiber grating.

3. In the LPG case, the process is different in the sense that co-propagating fiber modes are coupled by the grating. The LPG operation process is taking place in the entire fiber cross section. The LPG operation is based on the coupling of a core mode with the possible cladding propagating modes. Inherently, two possible single-mode fiber simulation models are to be considered: (a) two layers (core and cladding or cladding and environment) and (b) three layers (core, cladding and environment). As a consequence, into the more or less broad emission spectrum of a light source connected at one end of the fiber, there will appear several absorption bands with the strength and bandwidth depending on how much the transverse intensity distributions of core mode and cladding modes are overlapping, the values of "DC" and "AC" coupling coefficients depending on this mode superposition. The resulting absorption bands are usually observed at the other fiber end. The main task of LPG simulation consists in defining the peaks and bandwidths of these absorption bands appearing in the test light source transmission spectrum. The spectral shifts of absorption peaks and bandwidth broadenings can be correlated with grating period changes imposed by simple or simultaneous mechanical or thermal loads applied on the fiber grating. It becomes possible to correlate any modification of environment refraction index modification induced chemically or thermally by external factors. The spectral peak shifts and bandwidth broadenings of this absorption bands are to be evaluated.

Nevertheless, there are several steps to be accomplished in development of an accurate FBG or LPG simulation model, based on which a practical simulation algorithm can be defined. The first steps are identical for FBG and LPG simulation cycles. The first two identical steps of FBG and LPG simulations consist of:

- STEP 1—the usual gathering of input data, meaning core and cladding diameters, core and cladding refractive index values, to which the environment refractive index has to be added in LPG case and is only informal for FBG model. Any data concerning the geometry of the fiber grating has to be considered in this stage. For example, if fiber grating is supposed to be bent, or elongated, or longitudinally compressed or not.

- STEP 2—evaluation of fiber core effective value of the refractive index. This task is achieved by graphically or numerically solving the dispersion Eq. (4) for b and using Eq. (5). For more strictness, the confinement factor can be calculated using (6). The results of Step 2 consist of variation curves with wavelength of core effective refractive index, normalized frequency V and, eventually, of confinement factor$_\Gamma$.

In this stage, the FBG and LPG simulation cycles separate into different ways of evolution. In the FBG case:

- STEP 3 FBG—evaluation of fiber short-period grating reflectivity spectrum in the domain including the Bragg wavelength by solving the system of differential equations defined from coupled-mode theory applied for core counter-propagating modes, i.e. using Eqs. (39)–(42). The obtained reflectivity spectrum will depend on the grating length, period and if it is uniform or has a variable period according to a predefined law on z along the grating (sine, sinc, positive tanh or Blackman) but keeping a constant amplitude of δn_{eff}, this being the chirping technique, or it is apodized, meaning that the period is constant and the amplitude of δn_{eff} is defined by a variation law on z as the argument (also sine, sinc, positive tanh or Blackman functions are applicable). Once the Bragg grating reflectivity spectrum is obtained, it is possible to correlate its spectral shift with mechanical or thermal load applied on the FBG device, meaning to use it as a sensor. FBG chirping or apodization is used for smoothing the reflectivity spectrum wings.

In this moment, two ideas have to be underlined:

- The matrix transfer theory, which is based on dividing the fiber grating into a number of segments of short length (in comparison to the propagating light wavelength), the light propagating through these segments, the output signal (power) of one being the input for the next one and so on, the input of the first segment being the initial conditions for coupled-mode differential equations. Finally, in the matrix transfer theory, an iteration equation is defined, and solving it leads to the reflectivity spectrum. For FBG, coupled-mode and matrix transfer theories conduct to similar results.

- Tilted FBG consisting of a Bragg grating with pitches having an angle with z fiber axis represents an attempt to couple the core specific processes to the environment via cladding. The analysis of tilted FBG is beyond the purposes of this Chapter.

http://dx.doi.org/10.5772/63890

The LPG case:

- STEP 3 LPG—evaluation of refractive index values for the possible cladding propagation modes and of resonance peak wavelength of absorption bands created into the grating transmission band. This task can be accomplished by using a two layers or three layers model of the optic fiber for solving the dispersion Eq. (4) in order to define the effective values of cladding possible propagation modes. The Two Layers model means to consider the fiber itself as a core placed into an infinite cladding and to solve Eq. (4). It is a modified procedure applied at STEP 2. The two layers model is an approximation. The more accurate three layers model means to solve a modified version of dispersion equation obtained by a complicated algebra calculation taking into account the refractive index values of core, cladding and environment. This procedure is continued by evaluation of the peak wavelengths of the absorption bands created in the LPG transmission spectrum using the resonance relation Eq. (16). The differences observed between simulation results obtained using the Two or Three Layers models are of 5-10%, depending on the computational hardware and software capacity. These differences are observed for cladding modes propagating near the core.
- STEP 4 LPG—evaluation of coupling coefficients and the bandwidths of the corresponding absorption bands created in the LPG spectrum and consequently the entire transmission spectrum simulation. STEPS 3 and 4 LPG can be used for simulation of absorption bands peaks shifting and bandwidth broadening corresponding to applying mechanical or thermal loads on the LPG device or environment refractive index variation, i.e. the use of LPG as a sensor device.

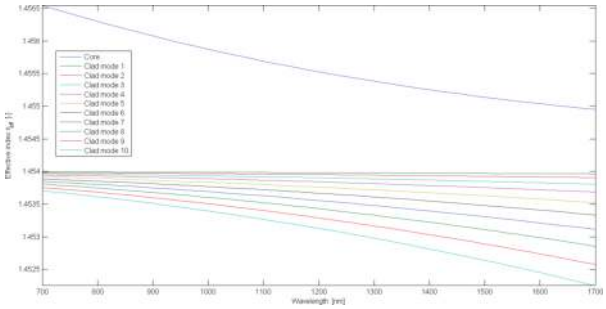

Figure 4. The variations of core and clad refractive indices versus propagating radiation wavelength.

In the following, several examples of FBG and LPG optical characteristic simulations developed in the above-described steps are presented. In the FBG case, the presented examples are obtained for uniform, chirped or apodized, the grating reflectivity being the main target. For LPG, its transmission characteristics are to be simulated. In the presented examples, simulation was performed considering the geometry and refractive index core and cladding values characteristic for Fibercore SM750 optical fiber (core radius 2.8 μm, $n_{co} = 1.4575$, cladding radius 62.5 μm, $n_{cl} = 1.4545$). Fibercore SM750 optical fiber is commonly used as host for FBG or LPG.

For both FBG and LPG sensors design, the first step consists in simulation of core and cladding effective refraction indices of propagation modes. **Figure 4** displays the results obtained in simulation of core and cladding refractive indices variations versus the wavelength of light propagating through the fiber. There are analyzed possible values of refractive index for which the radiation modes can propagate through the optic fiber.

Results obtained in the analyzed FBG cases are presented in **Figures 5-10**. The primary task accomplished by simulation consists in defining the variation of the FBG reflectivity with wavelength around the Bragg resonance wavelength. In simulation of chirped and/or apodized Bragg grating, for its period variation law, sine, sinc, positive tanh and Blackman profiles were considered.

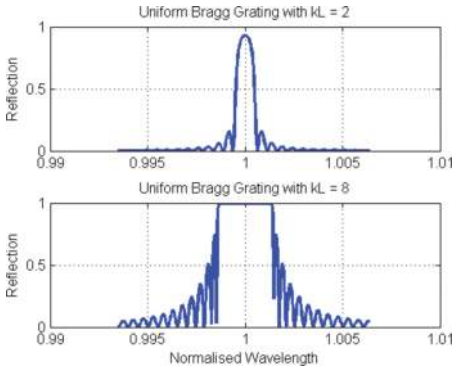

Figure 5. Variation of FBG reflectivity versus wavelength for a uniform Bragg grating displaying different grating strength *kL*. Length of the grating $L = 1$ mm, grating visibility $v = 1$, number of grating pitches $N = 10{,}000$, grating amplitude $\Delta n_{eff} = 1e{-}4$, design wavelength $\lambda_D = 1550$ nm.

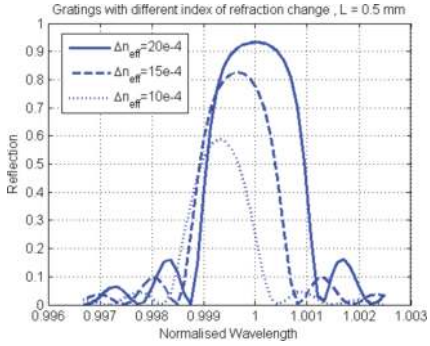

Figure 6. Effect of change in refractive indices on reflection spectra of uniform Bragg gratings. Length of the grating $L = 1$ mm, grating visibility $v = 1$, number of grating pitches $N = 10{,}000$, grating amplitudes 2206 = 20e−4, 15e−4 and 10e−4, design wavelength $\lambda_D = 1550$ nm.

http://dx.doi.org/10.5772/63890

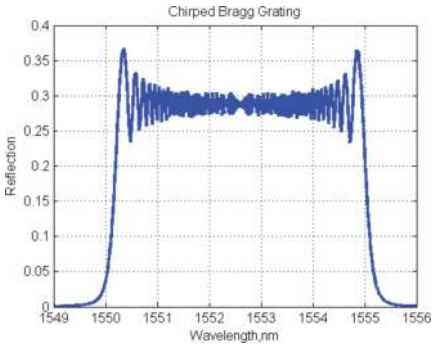

Figure 7. Reflection of a Gaussian profile chirped Bragg grating. Length of the grating L = 50 mm, grating visibility v = 1, number of grating pitches N = 10,000, grating amplitude = 20e−4, design wavelength λ_D = 1550 nm.

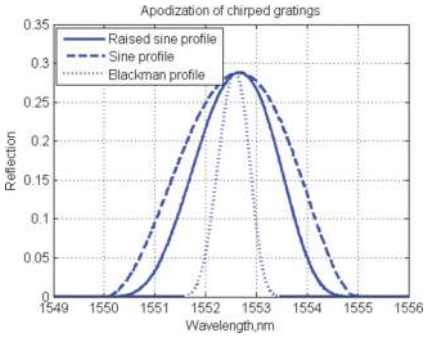

Figure 8. Apodization of a chirped grating using different profiles. Length of the grating L = 50 mm, grating visibility v = 1, number of grating pitches N = 10,000, grating amplitude Δn_{eff} = 20e−4, design wavelength λ_D = 1550 nm.

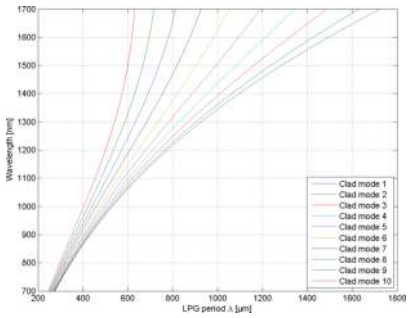

Figure 9. Variations of the resonance wavelength versus LPG period, calculated for the first 10 possible clad propagation modes. LPG length L = 75 mm, grating amplitude Δn_{eff} = 25e−4.

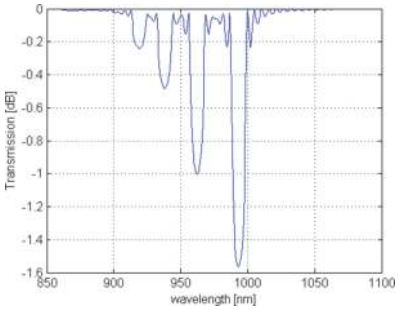

Figure 10. LPG transmission spectra simulated for an optic fiber in normal state. LPG period = 400 μm, LPG length L = 75 mm, grating amplitude Δn_{eff} = 25e−4.

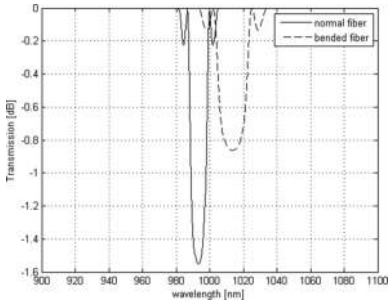

Figure 11. LPG transmission spectra simulated for a bent optic fiber in normal state. LPG period = 400 μm, LPG length L = 75 mm, grating amplitude Δn_{eff} = 25e−4.

Results obtained in the analyzed LPG cases are presented in **Figures 9–11**. In **Figure 9** are presented simulation results obtained regarding the variations of the resonance wavelengths of the absorption peaks in the LPG transmission spectra, peaks defined using (16)-the "second key task to be accomplished" in the design of LPG fiber sensors. In **Figures 10** and **11** are presented the LPG transmission spectra simulated for an unperturbed fiber and for a bent fiber.

4. Conclusions

The chapter refers to a broad research domain concerning the optic fiber and fiber grating physics. One of the two main purposes of the chapter consists in presenting the theoretical tools and simulation procedures used for analysis of optical properties of short-period FBG and fiber LPG. The second purpose of the chapter consists in providing the basics of simulation models. Examples of simulation results obtained using coupled-mode theory, verified using

the transfer matrix theory in the FBG case, are presented. The presented simulation results are in fairly good agreement with experimental and simulation results presented in literature.

Acknowledgments

This work was funded by Core Program, under the support of ANCS, project PN 16.40.01.02

Author details

Dan Savastru*, Sorin Miclos, Marina Tautan and Ion Lancranjan

*Address all correspondence to: j_j_f_l@yahoo.com

National Institute of Research and Development for Optoelectronics, Magurele, Ilfov, Romania

References

[1] A. Othonos, K. Kalli. Fiber Bragg gratings, fundamentals and applications in telecommunications and sensing. Boston: Artech House; 1999. 433 p. ISBN 0-89006-344-3

[2] A. Hongo, S. Kojima, S. Komatsuzaki. Application of fiber Bragg grating sensors and high speed interrogation techniques. Structural Control & Health Monitoring. 2005;12(3–4):269–282. doi:10.1002/stc.70

[3] L. Dong et al. Single-pulse Bragg gratings written during fiber drawing. Electronics Letters. 1993;29(17):1577–1578. doi:10.1049/el:19931051

[4] B.H. Lee, J. Nishii. Self-interference of long-period fibre grating and its application as temperature sensor. Electronics Letters. 1998;34(21):2059–2060. doi:10.1049/el:19981420

[5] S.W. James, R.P. Tatam. Optical fibre log-period grating sensors: characteristics and applications. Measurement Science and Technology. 2003;14(5):R49–R61. doi: 10.1088/0957-0233/14/5/201

[6] J-L. Archambault, L. Reekie, P. J. Russel. 100-percent reflectivity Bragg grating reflectors produced in optical fibers by single excimer laser pulses. Electronic Letters. 1993;29(5):453–455. doi:10.1049/el:19930303

[7] Y-J Rao. In-fiber Bragg grating sensors. Measurement Science and Technology. 1997;8(4):355–375. PII: S0957-0233(97)72999-0

[8] S. A. Slattery, D. N. Nikogosyan. High intensity UV laser inscription of fiber Bragg gratings and comparison with other fabrication techniques. In: B. W. Bowe, et al.,

editors. Opto-Ireland 2005: Photonic Engineering; 5–6 Apr 2005; Dublin, Ireland. Bellingham, WA, USA: SPIE-Int Soc Optical Eng; 2005. p. 200–210. doi: 10.1117/12.601158

[9] C. G. Askins et al. Stepped wavelength optical-fiber Bragg grating array fabricated in line on a draw tower. Optics Letters. 1994;19(2):147–149. doi:10.1364/OL.19.000147

[10] K. Schroeder, W. Ecke, R. Mueller, R. Willsch, A. Andreev. A fibre Bragg grating refractometer. Measurement Science and Technology. 2001;12(7):757–764. doi: 10.1088/0957-0233/12/7/301

[11] G. Laffont, P. Ferdinand. Fiber Bragg grating-induced coupling to cladding modes for refractive index measurements. In: A.G. Mignani, H.C. Lefevre, editors. 14th International Conference on Optical Fiber Sensors; 11–13 Oct 2000; Venice, Italy. Bellingham, WA, USA: SPIE-Int Soc Optical Eng; 2000. p. 326–329. WOS:000167396300080

[12] G. Laffont, P. Ferdinand. Tilted short-period fibre-Bragg-grating-induced coupling to cladding modes for accurate refractometry. Measurement Science and Technology. 2001;12(7):765–770. doi:10.1088/0957-0233/12/7/302

[13] T. Erdogan. Fiber grating spectra. Journal of Lightwave Technology. 1997;15(8):1277–1294. doi:10.1109/50.618322

[14] R. Kashyap. Fiber Bragg gratings, 1st ed. London: Academic Press; 1999. 458 p. ISBN: 0124005608

[15] B.H. Lee, Y. Chung, W-T. Han, U-C. Paek. Temperature sensor based on self-interference of a single long-period fiber grating. IEICE Transactions on Electronics. 2000;E83C(3):287–292. WOS:000086147100004

[16] G. Keiser. Optical fiber communications, 3rd ed. Singapore: McGraw Hill; 1999. 688 p. ISBN: 0-07-232101-6

[17] A.W. Snyder, J.D. Love. Optical waveguide theory, 1st ed. New York, USA: Chapman & Hall; 1983. 738 p. ISBN: 0412099500

[18] K. O. Hill, Y. Fujii, D. C. Johnson, B. S. Kawasaki. Photosensitivity in optical fiber waveguides: application to reflection filter fabrication. Applied Physics Letters. 1978;32(10):647–649. doi:10.1063/1.89881

[19] G. Meltz, W. W. Morey, W.H. Glenn. Formation of Bragg gratings in optical fibers by a transverse holographic method. Optics Letters. 1989;14(15):823–5. doi:10.1364/OL.14.000823

[20] D. Marcuse. Theory of dielectric optical waveguides. 1st ed. New York: Academic Press; 1974. 257 p. doi: ISBN: 0124709508

[21] H. Tai. Simple numerical simulation of strain measurement. In: R.M. Wasserman, S.L. DeVore, editors. Conference on Electro-Optical System Design, Simulation, Testing,

and Training; 09–10 July, 2002; Seattle, USA. Bellingham, WA, USA: SPIE-Int Soc Optical Engineering; 2002. p. 13–24. doi:10.1117/12.451768

[22] R. Savastru, I. Lancranjan, D. Savastru, S. Miclos. Numerical simulation of distributed feed-back fiber laser sensors. In: V.I. Vlad, editor. 10th Conference on Optics—Micro- to Nanophotonics III (ROMOPTO); 03–06 Sep 2012; Bucharest, Romania. Bellingham, WA, USA: SPIE-Int Soc Optical Engineering; 2013. p. UNSP 88820Y. doi: 10.1117/12.2032724

[23] I. Lancranjan, S. Miclos, D. Savastru, R. Savastru, C. Opran. Numerical simulation of a laser - acoustic landmine detection system. In: T. Graf, JI. Mackenzie, H. Jelinkova, J. Powell, editors. Conference on Laser Sources and Applications; 16–19 Apr 2012; Brussels, Belgium. Bellingham, WA, USA: SPIE-Int Soc Optical Engineering; 2012. p. 843315. doi:10.1117/12.922158

[24] I. Lancranjan, S. Miclos, D. Savastru, A. Popescu. Numerical simulation of a DFB-fiber laser sensor (II)—theoretical analysis of an acoustic sensor. Journal of Optoelectronics and Advanced Materials. 2010;12(12):2456–2461. WOS: 000286043000019

[25] I. Lancranjan, S. Miclos, D. Savastru. Numerical simulation of a DFB-fiber laser sensor (I). Journal of Optoelectronics and Advanced Materials. 2010;12(8):1636–1645. WOS: 000281695300002

[26] S. Miclos, D. Savastru, I. Lancranjan. Numerical simulation of a fiber laser bending sensitivity. Romanian Reports in Physics. 2010;62(3):519–527. WOS: 000287272300008

[27] S. Miclos, D. Savastru, R. Savastru, I. Lancranjan. Design of a smart superstructure FBG torsion sensor. In: J.L. Sanchez Rojas, R. Brama, editors. Conference on Smart Sensors, Actuators, and MEMS VII 1st SPIE Conference on Cyber-Physical Systems; 04–06 May 2015; Barcelona, Spain. Bellingham, WA, USA: SPIE-Int Soc Optical Engineering; 2015. p. 95172B. doi:10.1117/12.2188231

[28] D. Savastru, S. Miclos, R. Savastru, I. Lancranjan. Numerical analysis of a smart composite material mechanical component using an embedded long period grating fiber sensor. In: J.L. Sanchez Rojas, R. Brama, editors. Conference on Smart Sensors, Actuators, and MEMS VII 1st SPIE Conference on Cyber-Physical Systems; 04–06 May 2015; Barcelona, Spain. Bellingham, WA, USA: SPIE-Int Soc Optical Engineering; 2015. p. 95172B. doi:10.1117/12.2188231

[29] K. O. Hill, B. Malo, F. Bilodeau, D. C. Johnson. Photosensitivity in optical fibers. Annual Review of Materials Science. 1993;23:125–157. WOS: A1993LQ76400005

[30] R. J. Campbell, R. Kashyap. The properties and applications of photosensitive germanosilicate fiber. International Journal of Optoelectronics. 1994;9(1):33–57. WOS: A1994PL77900004

[31] P. St. J. Russell, J.-L. Archambault, L. Reekie. Fiber gratings. Physics World. 1993;6(10): 41–46. WOS: A1993MB88600025

[32] I. Bennion, J. A. R. Williams, L. Zhang, K. Sugden, N. J. Doran. UV-written in-fiber Bragg gratings. Optical and Quantum Electronics. 1996;28(2):93–135. doi: WOS: A1996TV07200001

[33] V. Mizrahi, J. E. Sipe. Optical properties of photosensitive fiber phase gratings. Journal of Lightwave Technology. 1993;11(10):1513–1517. doi:10.1109/50.249888

[34] M. Born, E. Wolf. Principles of optics. 7th ed. Cambridge, UK: Cambridge University Press; 1999. 952 p. ISBN: 0521642221

[35] A. Yariv. Coupled-mode theory for guided-wave optics. IEEE Journal of Quantum Electronics. 1973;QE-9(9):919–933.

[36] J. E. Sipe, L. Poladian, C. M. de Sterke. Propagation through nonuniform grating structures. Journal of the Optical Society of America A-Optics Image Science and Vision. 1994;11(4):1307–1320. doi:10.1364/JOSAA.11.001307

[37] H. Kogelnik. Filter response of nonuniform almost-periodic structures. Bell System Technical Journal. 1976;55(1):109–126. doi:10.1002/j.1538-7305.1976.tb02062.x

[38] K.O. Hill. Aperiodic distributed-parameter waveguides for integrated optics. Applied Optics. 1974;13(8):1853–6. doi:10.1364/AO.13.001853

[39] B. Malo, S. Theriault, D. C. Johnson, et al. Apodised in-fiber Bragg grating reflectors photoimprinted using a phase mask. Electronics Letters. 1995;31(3):223–225. doi: 10.1049/el:19950150

[40] F. Ouellette. Dispersion cancellation using linearly chirped Bragg grating filters in optical waveguides. Optics Letters. 1987;12(10):847–9. doi:10.1364/OL.12.000847